Microstructure, Hardness Profile and Tensile Strength in Welds of AA6013 T6 Extrusions

A comparison of gas tungsten arc and laser beam welds reveals the characteristics unique to each process

BY L. A. GUITTEREZ, G. NEYE AND E. ZSCHECH

Age-hardenable Al-Mg-Si alloys are of special interest for structural components of airplanes. The AA6013 alloy is a high-strength 6XXX series alloy and offers a strength 25% higher than AA6061 in the solution heat-treated and artificially aged (T6) condition (Ref. 1). This is caused by the presence of very fine, needle-shaped ß" (Mg_2Si) precipitates along <100> directions in the aluminum matrix (Ref. 2).

Alloy AA6013 is easily welded by conventional arc welding processes (*e.g.*, gas tungsten arc welding, GTAW), as well as by high-energy-density processes (*e.g.*, laser beam welding, LBW). However, some physical properties, which are inherent to all aluminum alloys, have to be considered during welding. In comparison to steel, the high thermal conductivity of aluminum alloys requires the use of higher heat input for welding. This is realized by a greater welding current during GTAW of aluminum alloys (Ref. 3). One of the main problems associated with LBW of aluminum alloys is the high surface reflectivity. In particular, the threshold intensity for the development of a keyhole is much higher for aluminum than for steel (Ref. 4). Finally, aluminum alloys, and particularly the heat-treatable alloys, are sensitive to weld cracking. This phenomenon can be avoided by proper filler and base metal alloy selection and adequate filler metal dilution (Ref. 3).

The resulting properties of the aluminum joints are caused by both the chemical composition and the microstructure in the fusion zone (FZ) and heat-affected zone (HAZ). Composition and microstructure are controlled by the alloying constituents of the base metal and of the filler metal, as well as by the welding process and welding parameters. In particular, vaporization loss from the weld pool surface, interdiffusion between the base metal and the weld pool, as well as decomposition and precipitation mechanisms in the welded joint, depend on the kind and amount of alloying elements.

During welding, a volatilization of alloying elements like Mg may occur. Vaporization loss of alloying elements may influence the mechanical properties of the welded joint by affecting the weld pool chemistry (Ref. 5).

The relative rates at which dissolution and precipitation occur with different solutes depend on the respective diffusion rates, solubilities, and alloying contents. Magnesium, silicon and copper, which are principally involved in the precipitation hardening reaction of AA6013, have relatively high rates of diffusion in aluminum (Ref. 2).

Prior investigators have reported that the heat input of welding causes a severe softening in the HAZ. This loss of strength is caused by reversion (dissolution) of the strengthening β" (Mg_2Si) phase and by formation and growth of nonstrengthening β' (Mg2Si) precipitates. It is a major problem in engineering design, and may be significantly affected by welding parameters, such as welding current and welding speed (Refs. 6, 7).

Although these problems are inherent in the metallurgy of the Al-Mg-Si alloys, existing joining difficulties seem to be solvable by choosing advanced welding techniques, as well as optimized filler metal composition and welding parameters.

In order to improve the mechanical integrity of Al-Mg-Si weldments, it would be desirable to study the microstructure of the FZ and of the HAZ, as well as the residual stress distribution. The present study was performed in order to show differences in microstrucure, hardness profile and tensile strength of gas tungsten arc (GTA) and laser beam (LB) welded AA6013-T6 extrusions. In addition, grain boundary liquations and hot tearing are discussed.

KEY WORDS

Microstructure
Hardness Profile
Tensile Strength
6013 T6 Extrusions
GTAW
Laser Beam Welds
Al-Mg-Si Alloys
HAZ
Fusion Zone
Fracture Surface

Extrusion Material and Joint Design

The material used during the investigation was the precipitation-hardenable AA6013 aluminum alloy, which contains magnesium, silicon and copper as the major alloying additions. The composi-

L. A. GUITTEREZ is with Colorado School of Mines, Center for Welding and Joining Research, Golden, Colo. G. NEYE and E. ZSCHECH are with Daimler-Benz Aerospace Airbus GmbH, Bremen, Germany.

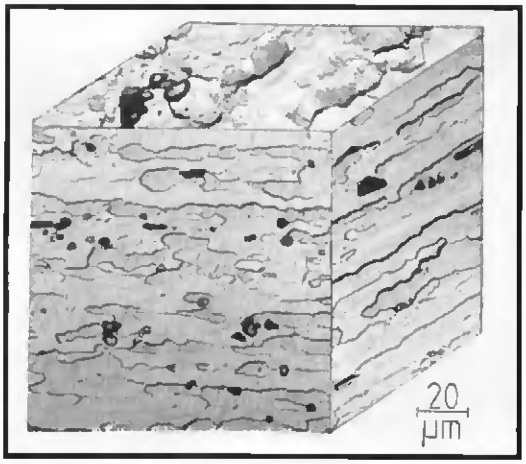

Fig. 1 — Microstructural cube of AA6013-T6 as-extruded material with $Al_{15}(Fe,Mn)_3Si$ and Mg_2Si precipitations (etching: 50 mL H_2O, 10 mL HF, 15 mL HCl, 25 mL HNO_3; etching time 2 min).

tion limits of the alloy are listed in Table 1. Extrusion profiles produced by Vereinigte Aluminium-Werke AG (VAW, F. R. Germany) were solution heat treated, quenched and subsequently artificially aged to the T6 condition (peak strength).

The microstructure of the as-extruded material can be seen in Fig. 1. It represents a typical precipitation-strengthened aluminum alloy in the T6 condition. The observed phases are cubic $Al_{15}(Fe,Mn)_3Si$ primary precipitations (light in Fig. 1) and Mg_2Si secondary precipitations (dark in Fig. 1).

Due to the extrusion process and the subsequent recrystallization, the grain size ranges from very coarse to fine with respect to location. In particular, very coarse recrystallized grains are located in the near-surface region of the as-extruded material, and a relatively fine-grained microstructure exists in the bulk of the material — Fig. 2. The coarse grains are possibly a result of a certain combination of nonuniform deformation, recrystallization temperature and time spent at the recrystallization temperature. The coarse-grained region of the material is expected to be more susceptible to liquation cracking in the partially melted zone (PMZ) of the welded joint because a higher concentration of low-melting segregates at the grain boundaries.

Table 1 — Limits of Chemical Composition of the AlMg5iCu Alloy AA6013 (Ref. 1)

Chemical Element	Composition Limits (wt-%)
Si	0.6–1.0
Fe	0.5
Cu	0.6–1.1
Mn	0.2–0.B
Mg	0.8–1.2
Cr	0.1
Zn	0.25
Ti	0.1
Others, each	0.05
Others, total	0.15
Aluminum	Remainder

The joint design and the fusion zone for GTAW are shown in Fig. 3. The discussion of the GTA-welded samples will concentrate on bead 1 because the mechanical properties are conducted on this particular area of the extrusion profile. In the case of LB welding, square-groove butt joints were produced using extruded flat profiles with 3 mm (0.12 in.) thickness.

Welding Process

Gas Tungsten Arc Welds

The gas tungsten arc (GTA) process has proved for many years to be suitable for welding aluminum. The special direct current electrode negative (DCEN) polarity was used for this particular study. In this method, the welding current can be pulsed between different levels for short or long time intervals (Ref. 8).

During this pulsing mode, parts of the fusion zone can be heated up to the melting point during the peak pulse. Afterward, they are allowed to cool and solidify during the low background current period. Overlapping weld spots may be observed after welding with low frequency pulsing. From Fig. 4, one can see schematically the relative dimensions of the weld along with the overlap area.

Pulsed GTA-DCEN welding results in the following advantagous characteristics of the final welded structure:

- Narrow bead due to reduction in volume of melted base metal.
- Relatively good joint penetration.
- Fast solidification rate during the low-current phase.

The butt joints were produced with a Squarearc 400 machine, using a tungsten electrode (diameter 2.4 mm, 27-deg total cone angle with 0.5-mm tip). The process parameters are listed in Tab. 2.

Laser Beam Welds

Laser beam welding of aluminum is an efficient technology for many applications because of the following attractive features of this process:

- Small amount of fused material (narrow weld bead).
- Small heat-affected zone.
- Reduced shrinkage due to minimum heat input.
- Precisely located weld bead (due to narrow high-energy laser beam).

In this study, a Rofin Sinar RS 10000 CO_2 laser with a power of 7 kW was used at Bremer Institut fur Angewandte Strahltechnik (BIAS). The focus optics consisted of a series of water-cooled reflecting copper mirrors. The process parameters are listed in Table 2.

Results and Discussion

Microstructure

The three main regions that exist in welded aluminum alloys are the fusion zone (FZ), the partially melted zone (PMZ) and the heat-affected zone (HAZ). These regions are categorized by the temperature experienced during the welding process. They may be characterized in the following manner:

Fusion zone: completely melted during welding, maximum temperature above the liquidus temperature of the alloy.

Grain structure developed by epitaxial growth, competitive growth (columnar grains), and many times followed by the formation of equiaxed grains.

Solidification cracking or hot tearing (typically along the center of the weld or at terminator crackers).

Partially melted zone: partially melted during welding, maximum temperature range between eutectic temperature and liquidus temperature of the alloy.

Extensive segregation of the eutectic phase (low-melting-point segregate) at the grain boundaries.

Low ductility (hard and brittle eutectic phase).

Table 2 — Process Parameters of the GTA-DCEN and LB Welding

Process Parameter	GTA-DCEN Welding	LB Welding
Welding speed (mm/s)	2	100
Shielding gas	Ar	He
Gas flow (L/min)	14	15
Filler metal	AA4043 (AlSi5)	AA4043 (AlSi5)
Wire diameter (mm)	1.2	1.2
Wire feed	mechanized	mechanized
Wire feed rate (mm/s)	50	40

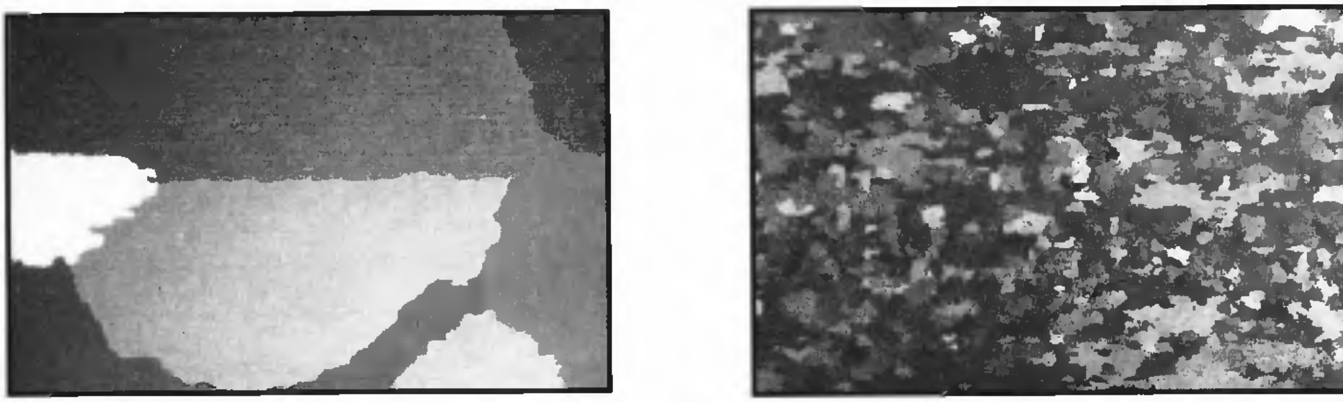

Fig. 2 — Planar view showing the variation in recrystallized grain size (etching of Fig. 1). A — On the surface of the as-extruded profile; B — transverse section through the bulk material.

Subsolidus cracking and liquation cracking (adjacent to the fusion zone).

Heat-affected zone: not melted during welding, maximum temperature below the eutectic temperature of the alloy.

Softening of precipitation-hardenable aluminum alloys (by full or partial reversion of GP zones and formation of incoherent precipitations, often described by dissolution and coarsening of particles).

Each of those zones can be further divided into more specific regions (e.g., Ref. 6).

GTA Welds

Figure 5 shows clearly the FZ and the PMZ (dark band in Fig. 5, near the weld interface) of a welded joint produced by GTAW. The microstructural changes in the HAZ, which are caused by the welding process, can only be seen by transmission electron microscopy (Ref. 9).

The microstructure of the FZ is characterized by columnar dendrites (Fig. 6) that were observed to be coarser near the weld interface than in the center of the weld. Micrographs of metallographic transverse sections provide a good indication of the solidification conditions — Figs. 6, 7. The subgrain structure is finer at the weld centerline and coarser near the weld interface because of the different cooling rates in these regions. The coarse columnar grains near the weld interface are due to directional cooling and, consequently, by different solidification conditions compared to the center of the weld. There exists a thermodynamically preferred direction of grain growth, the so-called "easy growth direction," which is <100> in f.c.c. Al alloys. On the other hand, the kinetics of grain growth is also influenced by the direction of the temperature gradient. Thermodynamic and kinetic considerations for heterogeneous nucleation, aided by constitutional supercooling at high heat input and welding speed, as well as for columnar grain growth are discussed in Ref. 6. In general, slow cooling during solidification, *i.e.*, a relatively long time available for coarsening results in large dendrite arm spacings. In this configuration, the total surface energy is reduced.

The PMZ with a coarse grain structure in the base material is seen near the weld interface — Fig. 7. Due to the recrystallization of the original extrusion microstructure, extremely large grains are observed down to a depth of 1 mm (0.04 in.) below the surface. The grain boundaries of the large recrystallized grains were probably liquated during welding — Fig. 8. The micrograph shows highly decorated grain boundaries. Grain boundary liquation occurs during the welding process, when low-melting segregates (precipitation-hardenable alloys like AA6013 contain a relatively large amount of alloying additions available to form eutectic phases) have accumulated at the grain boundaries during production of the extruded material, and they are melted due to the heat transfer during welding. In addition, diffusion takes place in the course of the welding process.

The composition within the grain boundaries in the PMZ were determined

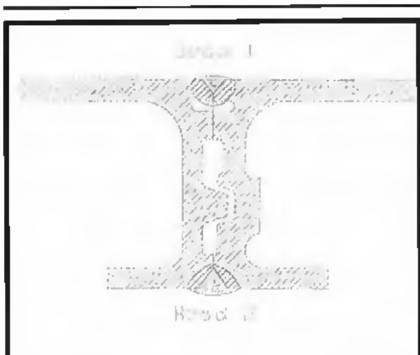

Fig. 3 — Joint design for GTAW of extruded profiles.

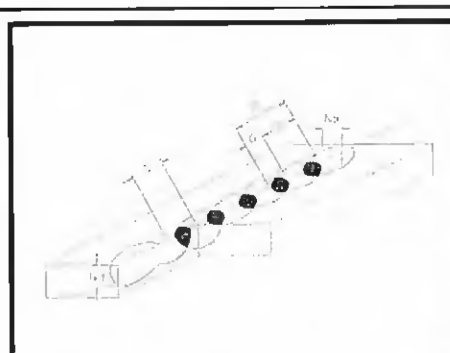

Fig. 4 — Three-dimensional scheme of the overlap areas produced during GTA-DCEN welding. B = Maximum length of the fused spot; Nb = maximum width of the fused spot; Nd = maximum penetration depth of a fused spot; O = length of overlap (welding direction); S = distance between fused spots.

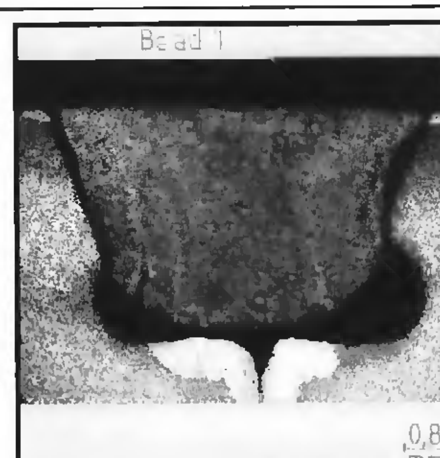

Fig. 5 — Macrosection of a GTA welded joint (etching of Fig. 1).

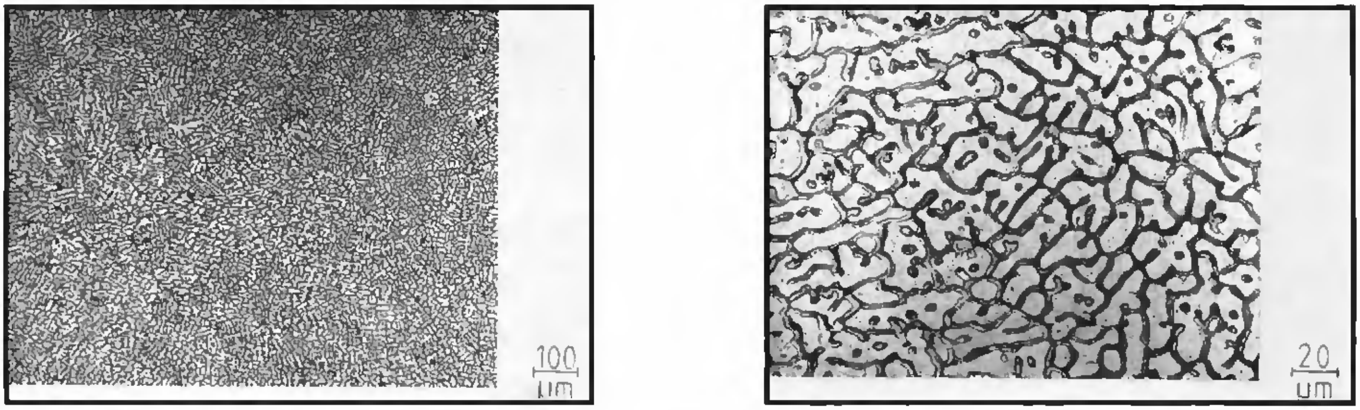

Fig. 6 — Dendritic structure near the center of a GTA-welded joint of AA6013-T6 extrusions, different magnifications (etching of Fig. 1).

by electron-probe microanalysis using wavelength-dispersive x-ray spectroscopy and by a transmission electron microscope using energy-dispersive x-ray spectroscopy. The results of both techniques have shown that the grain boundaries are composed mainly of Mg and Si (Ref. 9). The actual stoichiometry of the phase involved was difficult to determine, but, due to the concentrations of Mg and Si, the precipitation phase Mg_2Si is very likely.

Changes in content, dimension and morphology of Mg_2Si precipitations that cause the different hardnesses in the three regions of the HAZ of GTA welded samples (see below), are not resolvable with light microscopy and scanning electron microscopy (SEM). That is due to the sub-micron scale of the efficient precipitation hardening process (decomposition, formation of GP zones and metastable β′ phases).

LB Welds

The microstructure in the FZ of LB welds consists of fine subgrains (characterized by close spacing between the dendrite arms). In contrast, long columnar grains were observed near the weld interface. Figure 9 shows the dendritic microstructure near the center of the FZ of a transverse section.

Similar to GTA welded samples, the grain boundaries of large recrystallized grains are melted during the welding process, but only to a smaller extent. Small amounts of grain boundary liquation could be observed near the weld interface — Fig. 10.

The extent of the FZ in LB-welded samples is in general not as large as in GTA-welded samples.

Hardness Profiles

Hardness profiles were used to characterize the strength in the different zones across the welded joint. All hardness measurements were taken after sufficient natural aging time (about 100 h).

GTA Welds

The FZ width of the GTA-welded joints was 5 mm (0.2 in.), determined from macrographs of transverse sections. The extent of the material influenced by the welding (*i.e.*, FZ and HAZ) was determined from hardness profiles — Fig. 11. It was about 30 mm (1.2 in.). The maximum hardness is measured in the base material with $HVN_{0.3}$ 130, the minimum hardness in the HAZ 2, *i.e.*, 2–5 mm (0.08–0.2 in.) from the weld interface, with $HVN_{0.3}$ 80 (Ref. 9).

Fusion zone, HAZ and base metal are characterized by different hardness values. The HAZ can be subdivided into three different regions as follows:

HAZ 1 (fully reverted region). Dissolution of β″ precipitations, supersaturized solid solution (fast cooling rate), natural aging after a sufficient time (about 100 h)

HAZ 2 (overaged region). Coarsening of β′ precipitations (local hardness minimum).

HAZ 3 (Partially overaged region). Minor growth of precipitations (reduced hardness in comparison with the base material).

The hardness minimum in the HAZ 2 is the result of a sequence of reactions occuring in the HAZ of AA6013-T6 welds: dissolution of β″ (Mg_2Si), precipitation of β′ (Mg_2Si) and subsequent natural aging.

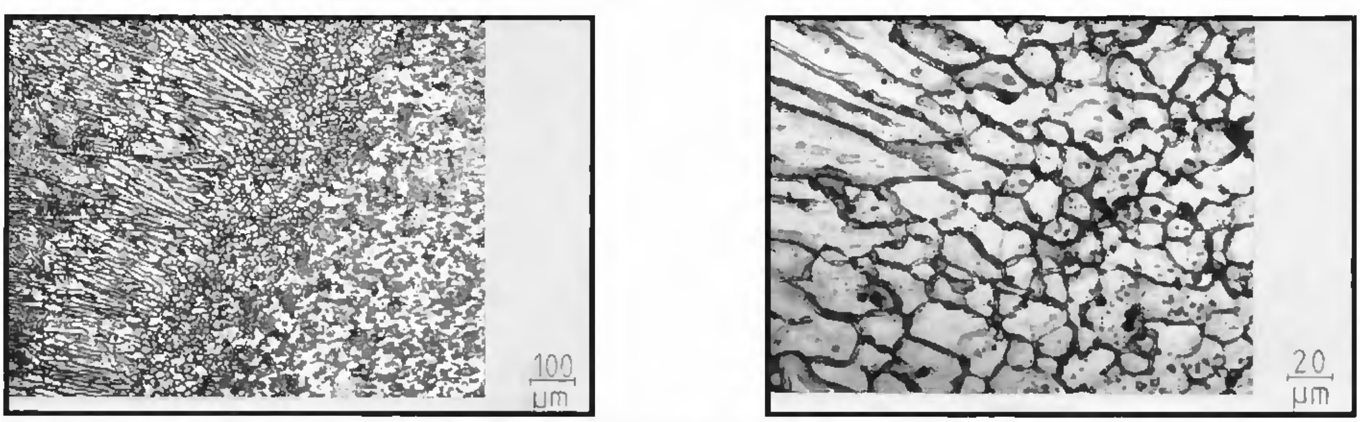

Fig. 7 — Transverse section through a GTA welded joint of AA6013-T6 extrusions, showing the partially melted zone and coarse columnar grains near the weld interface, different magnifications (etching of Fig. 1).

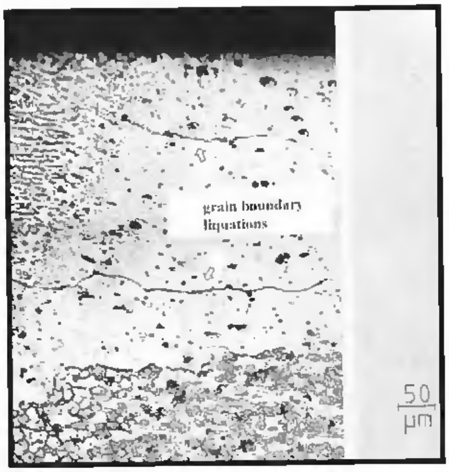

Fig. 8 — Grain boundary liquations in the partially melted zone of a GTA welded joint of AA6013-T6 extrusions (etching of Fig. 1).

These processes are similar in all 6XXX alloys (Ref. 10).

LB Welds

The FZ width of the LB-welded joints was about 2 mm (0.08 in.), determined from macrographs of transverse sections. The hardness profiles of LB welds are somewhat similar to those found in GTA-welded samples. One significant difference is the extent of the weld zone (*i.e.*,FZ and HAZ), which has a total width of only 6 mm (0.24 in.) for the LB-welded samples — Fig. 12. The local minimum in the HAZ 2 is as well defined, and the absolute minimum ($HVN_{0.3}$ 80) is localized in the FZ (Ref. 9).

Tensile Strength

The weld beads for all samples were machined (*i.e.*, reinforcement removed) and tested in the long transverse (L-T) direction. The test samples were in the as-welded condition.

GTA Welds

Due to the welding process, an approximate 40% decrease in ultimate tensile strength (UTS) was observed (from 420 MPa before to 246 MPa after welding). All failures occured in HAZ 2 approximately 4 mm (0.16 in.) from the weld interface. This region has been defined as the overaged region. The tensile test results are in coincidence with the minimum of the hardness profile.

LB Welds

Due to the welding process, an approximate 35% decrease in UTS occurred (from 420 MPa before to 275 MPa after welding). All failures occurred in the FZ, which confirms the results of the hardness profiles discussed previously. Another possible reason for the fracture in the FZ could be the higher solidification cracking sensitivity of the LB welded joints (different weld pool chemistry with lower Si content).

Comparison of UTS Results (GTAand LB Welds)

The data were analyzed using statistical algorithms in order to make the conclusions from the experimental values more objective. For the comparison of two average values, the t-test was used, for the comparison of two variances the F-test (Ref. 11). From this statistical significant test on the UTS results, it follows with more than 95% confidence that the tensile strength of the LB welds was higher than those of the GTA welds.

Fracture Surface

GTA Welds

The fracture surface characterized by SEM analysis showed dimples, which are typical features of a ductile transcrystalline fracture — Fig. 13. The examination of the fracture surface shows no weld porosity and no incomplete fusion. Therefore, the reason for the fracture in the HAZ 2 region is the "softening" of the base metal, caused by overaging of the material (coarsening of precipitates).

LB Welds

The results of the SEM analysis indicated that hot tearing had occurred in the entire sample. High cooling rates after welding and long columnar dendrites result in a highly crack susceptible state of liquid films during solidification. In Fig. 14, hot tears are evident. As in GTA welds, neither porosity nor incomplete fusion are visible.

Conclusions

Summarizing the experimental results, it can be seen that both GTAW and LBW processes are suitable for welding AA6013-T6 material. For the LB welds, a significantly higher tensile strength could be achieved than for GTA welds.

The most visible differences between LBW and GTAW are the geometry and the shape of the FZ. The extent of the weld zone is much larger for GTA-welded samples than for LB-welded samples. Metallurgical analysis has shown that the absolute minimum of the hardness profile is located in the HAZ 2 (overaged state of the material) in the case of GTAW, but in the FZ in the case of LBW. Therefore, the static tensile test results, *i.e.*, crack propagation in the HAZ 2 for GTA welded samples and in the FZ for LB welded samples, can be explained by the hardness profiles.

In the case of GTAW, the strength of the welded joints can be influenced by modified welding parameters, which reduce the "softening" of precipitation-hardenable materials in the HAZ 2 (re-

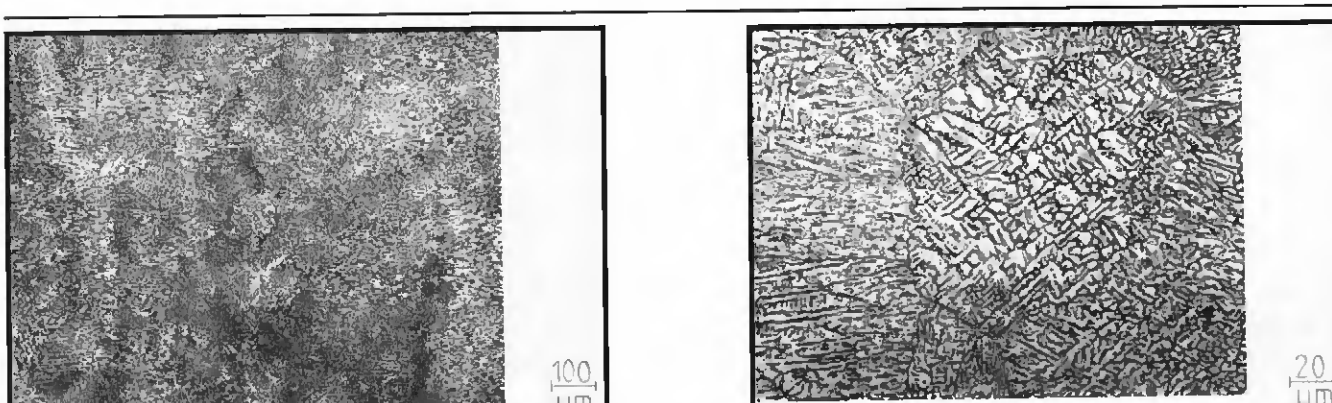

Fig. 9 — Dendritic structure near the center of a LB-welded joint of AA6013-T6 extrusions (etching of Fig. 1).

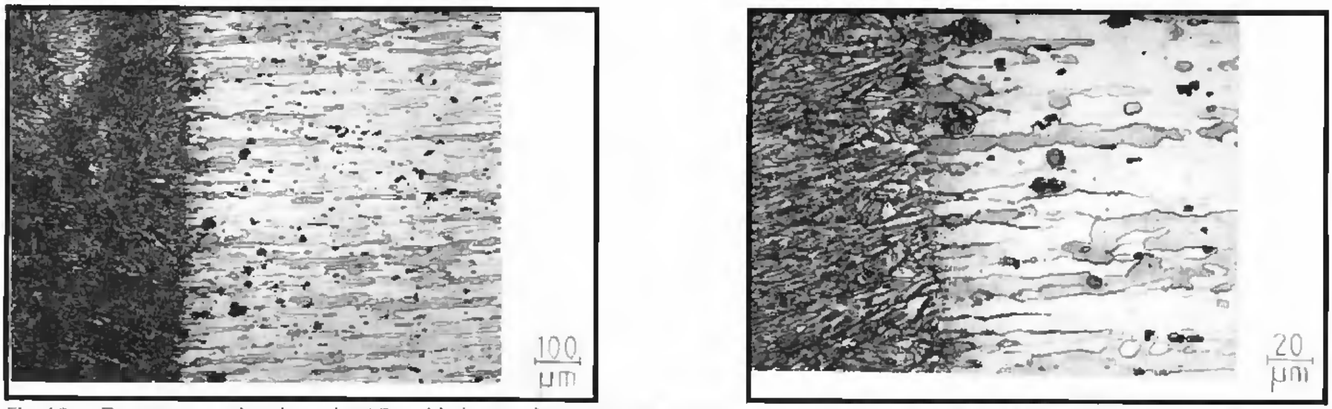

Fig. 10 — Transverse section through a LB-welded joint of AA6013-T6 extrusions. A — The heat-affected zone; B — the grain boundary liquations (etching of Fig. 1).

duced overaging). But the potential to improve the welding factor by parameter optimization is limited. In the case of LBW, the most efficient way to increase the welding factor is to optimize the filler metal. The real potential of the LB process for welding of aluminum materials will be demonstrated only with such filler metals that fit the base metal and the LB welding parameters (type of laser, welding speed).

Another important problem that has to be solved particularly for LB welding of aluminum alloys is the elimination of solidification cracking in the FZ. Solidification cracking occurs when high levels of thermal stress and solidification shrinkage are present (Ref. 5). In particular, the geometry for faster welding speeds produces a more elongated weld pool than for slower speeds. This type of weld pool geometry favors a columnar grain structure due to the faster solidification rate. The columnar grain structure is very susceptible to hot tearing due to their capability of accommodating solidification shrinkage strains. That means the hot tearing susceptibility is influenced by the welding parameters. On the other hand, hot tearing can be effectively controlled by the weld pool chemistry through the kind and amount of filler metal. In particular, the maximum of the hot tearing susceptibility of aluminum alloys exists at about 1 wt-% Si in the weld pool, and it is nearly zero for a Si content of more than 2 wt-% (Ref. 12). In our study, the Si content in the FZ of the GTA- and LB-welded joints were 1.2 and 2.4 wt-%, respectively. Therefore, an Al-Si filler metal with a higher Si content (e.g., eutectic composition) is proposed for LB welding of AA6013 parts in order to reduce the solidification crack susceptibility in the welded joints.

Since grain boundary liquation in the PMZ of the welded joints can be a problem, one has to prevent the generation of large recrystallized grains during the extrusion process.

Acknowledgments

The authors wish to thank Mr. Groß

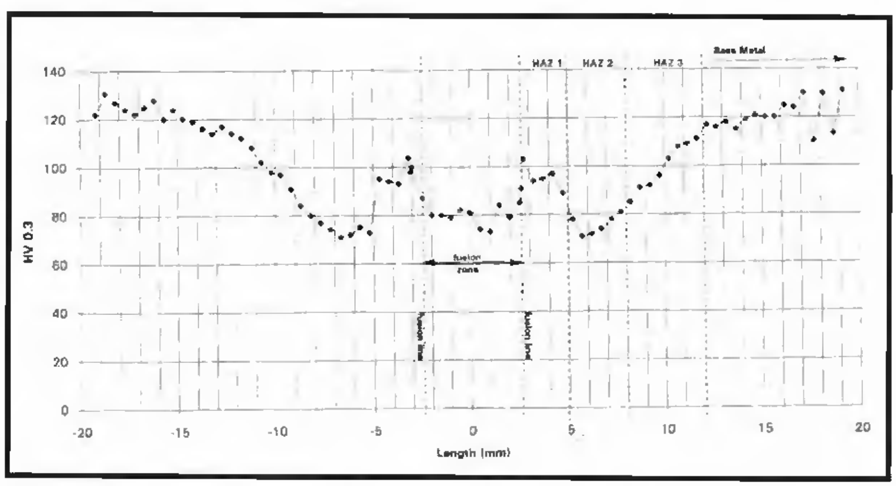

Fig. 11 — Macrograph and hardness profile (along centerline) of a GTA-welded joint (base metal AA6013-T6, filler metal AA4043).

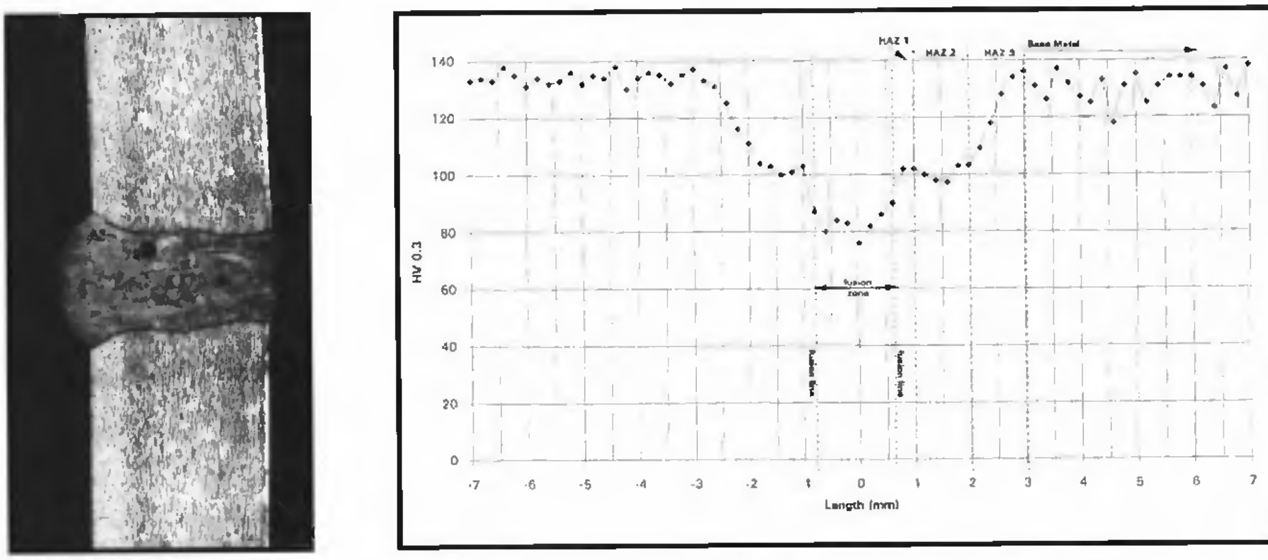

Fig. 12 — Micrograph and hardness profile (along centerline) of a LB-welded joint (base metal AA6013-T6, filler metal AA4043).

(Daimler-Benz Aerospace Airbus Bremen, FRG) and Mr. Heider (BIAS Bremen, FRG) for welding of the samples, as well as Mrs. Fior, Mr. Köch, Mrs. Pahling and Mrs. Radoy (Daimler-Benz Aerospace Airbus Bremen, FRG) for assistence in sample preparation and characterization. We are grateful to Mr. Weilke (now deceased) and Mr. Kolley (Daimler-Benz Aerospace Airbus, Bremen) for stimulating discussions.

References

1. Cieszlak, S. J. 1987. Alcoa Green Letter, Alcoa *Aluminum* Alloy 6013, Rough draft. Aluminum Company of America, Pittsburgh, Pa.

2. Hatch, J. E. 1984. Aluminum — *Properties and Physical Metallurgy.* ASM International, Materials Park, Ohio.

3. Martukanitz, R. P. 1994. Selection and weldability of heat-treatable aluminum alloys, *ASM Handbook — Welding, Brazing and Soldering,* Vol. 6., ASM International, Materials Park, Ohio.

4. Belforte, D. A. 1993. Laser materials processing — the next generation of applications. *Proc. 5th International Conference on Welding and Melting by Electron and Laser Beams,* La Baule, France, pp. 1–11.

5. Rapp, J., Glumann, C., Dausinger, F., and Hügel, H. 1993. The effect of magnesium evaporation in laser welding of aluminum alloys. *Proc. 5th International Conference on Welding and Melting by Electron and Laser Beams,* La Baule, France, pp. 275–282.

6. Kou, S. 1987. *Welding Metallurgy.* John Wiley & Sons, New York, N.Y.

7. Dumolt, S. D. 1983. *Metallurgical Transformations in the Heat-Affected Zone of Aluminum Alloys by Transmission Electron Microscopy.* Ph.D. dissertation, Carnegie-Mellon Univ., Pittsburgh, Pa.

8. *Welding Handbook* 1978. Vol. 2. American Welding Society, Miami, Fla.

9. Zschech, E., Neye, G., and Berek, H. 1995. Metallkundliche Untersuchungen an WIG- und LS - geschweißten AlMgSiCu-Strangpreßprofilen (Metallurgical study at GTA and LB welded AlMgSiCu extrusions). *Aluminium* 71(2): 220–224.

10. Myhr, O. R., and Grong, O. 1991. Process modeling applied to 6082-T6 aluminum weldments — part I: reaction kinetics. *Acta Metall. Mater.* 39: 2693–2702.

11. John, P. W. M. 1971. *Statistical Design and Analysis of Experiments,* Macmillan, New York, N.Y.

12. Cross, C. E., and Olson, D. L. 1986. Hot tearing model to assess aluminum weldability. *Proc. Conf. Aluminum Alloys.* Univ. of Virginia, Charlotte, Va., pp. 1869–1875.

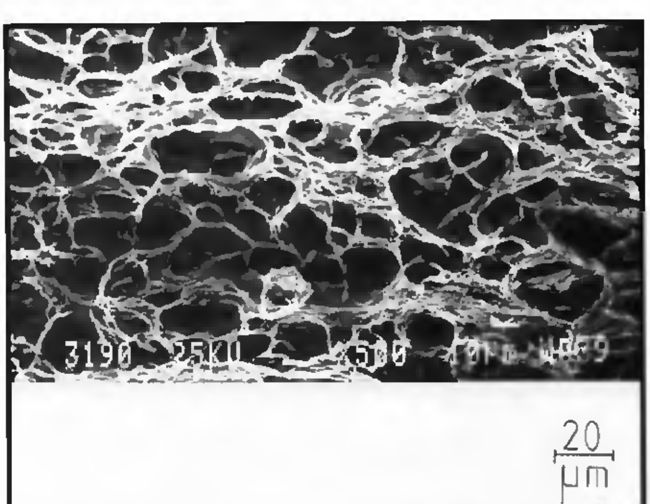

Fig. 13 — SEM micrograph of the ductile fracture surface in the overaged region of the heat-affected zone (HAZ 2) of a GTA-welded joint.

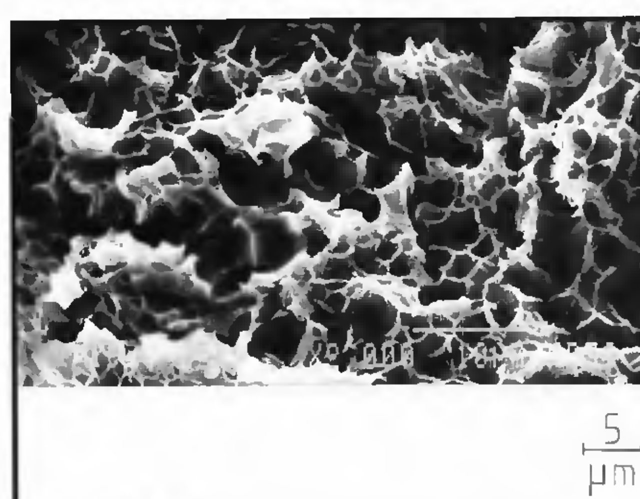

Fig. 14 — SEM micrograph of a fracture surface with hot tears in the fusion zone of a LB-welded joint.